More galaxies in the Local Volume imaged in $H\alpha$

Igor D. Karachentsev and Serafim S. Kaisin

Special Astrophysical Observatory, Russian Academy of Sciences, N. Arkhyz, KChR,
369167, Russia

ikar@sao.ru

ABSTRACT

We have carried out an $H\alpha$ flux measurement for 52 nearby galaxies as part of a general $H\alpha$ imaging survey for the Local Volume sample of galaxies within 10 Mpc. Most of the objects are probable members of the groups around Maffei 2/IC 342, NGC 672/IC 1727, NGC 784, and the Orion galaxy. The measured $H\alpha$ fluxes corrected for extinction are used to derive the galaxy star formation rate (SFR). We briefly discuss some basic scaling relations between SFR, hydrogen mass and absolute magnitude of the Local Volume galaxies. The total SFR density in the local ($z = 0$) universe is estimated to be $(0.019 \pm 0.003)M_\odot \ \mathrm{yr}^{-1} Mpc^{-3}$.

1. Introduction

Systematic measurements of $H\alpha$ fluxes in nearby galaxies within a fixed distance is one of the major techniques for determining the star formation rate (SFR) in the local universe. The presence of dwarf galaxies with extremely low luminosities in the Local Volume which are usually invisible at large distances, provides a unique opportunity for researching the SFR of a galaxy depending on its luminosity, structure, gas mass, and density of its environment in the broadest possible range of these characteristics. Thus it is essential that the observational program contains objects of all types and sizes in order to avoid the observational selection, distorting the interpretation of results.

Kraan-Korteweg & Tammann (1979) proposed to view an exemplary sample of 179 nearest galaxies with distances within 10 Mpc (the so-called LV sample). Later, Karachentsev (1994) replenished it with galaxies discovered from new redshift surveys. The updated sample constituted 226 galaxies. Later, Karachentseva & Karachentsev (1998,2000) and Karachentseva et al. (1999) undertook the all-sky search for nearby galaxies using plates of the POSS-II and ESO-SERC survey. A large number of new nearby dwarf galaxies of low surface brightness were found. A limiting magnitude of the survey was $B \simeq 17^m$ providing an essential completeness of the LV sample up to absolute magnitude $M_B \simeq -12.5^m$ within a distance of 8 Mpc. Their radial velocities were measured by Huchtmeier et al. (2000, 2001) during a subsequent HI-survey. Distances to many of the LV galaxies were first measured with high accuracy on the Hubble Space Telescope (HST) using the tip red giant branch (TRGB) method. The results of these international efforts were summarized in the Catalog of Neighboring Galaxies (CNG) (Karachentsev et al., 2004), consisting of 451 galaxies with distance estimates within $D < 10$ Mpc.

Different surveys of large areas of the sky in the optical and radio bands: SDSS (Abazajian et al. 2009), 2dF (Colless et al. 2001), 6dF (Jones et al. 2004), HIPASS (Zwaan et al. 2003), and ALFALFA (Giovanelli et al. 2005) have led to an essential increase of the Local Volume sample. The second version of the CNG (Karachentsev et al. 2011, in preparation) contains $N \simeq 790$ galaxies, i.e. more than four times that of the original list by Kraan-Korteweg & Tammann (1979). Such a representative sample, being registered

in the $H\alpha$ emission line, provides a detailed picture of star formation in the Local Volume during the recent time interval of $\sim$10 Myr.

Measurements of $H\alpha$ fluxes in nearby galaxies were performed by many authors. Their interest was normally fixed on objects of a certain type, for example, on spiral or irregular galaxies. A synopsis of publications, where the number of measured $H\alpha$ fluxes for the Local Volume galaxies was not less than 10, is presented in Table 1. The first column of the table contains a link to the paper, the second contains the number of LV galaxies imaged in $H\alpha$, and the third column reflects the nature of the sample (the morphological type of galaxies or their affiliation to a fixed group). The last row of the table summarizes the number of LV galaxies, which were observed in our program (Karachentsev et al. 2005; Kaisin & Karachentsev 2006, 2008; Kaisin et al. 2007; Karachentsev & Kaisin 2007), including the results of this paper. Unlike all previous observational programs, our $H\alpha$ survey of LV galaxies does not imply any selection of objects by morphological type, or their affiliation to a group. This has led to some unexpected results, in particular, to the detection of circumnuclear emission in isolated E/S0 galaxies (Moiseev et al. 2010).

As follows from the data above, so far there are 692 measurements of the $H\alpha$ flux available for 435 LV galaxies, i.e. a lot of galaxies were observed independently by different authors, which enables an estimate of the external error of the flux measurement. More than half of the $H\alpha$ data were obtained within the framework of two programs: Kennicutt et al. (2008) and our survey.

The degree of completeness of the Local Volume galaxy collection currently available remains quite ambiguous. New sky surveys reveal new nearby galaxies of both low and high surface brightness. Refinement of individual distances to galaxies leads to their inclusion or exclusion as LV members. Among $\sim$ 790 galaxies that are currently listed in the LV, there are objects with absolute magnitudes M_B ranging from -22^m to -4^m, i.e. their luminosities vary by more than seven orders of magnitude. Figure 1 presents the distribution of 572 galaxies situated within 8 Mpc according to their B-band absolute magnitude. The shaded areas on the left and right panels indicate numbers of galaxies that have been observed in $H\alpha$ and HI, respectively. The median absolute magnitude of the LV galaxies is -14^m. Measurements of the $H\alpha$ flux are carried out for 355 galaxies or 62% of the sample. As one can see, the current $H\alpha$ survey is almost complete on the bright half of the luminosity function, i.e. up to $M_B \simeq -15^m$. For a comparison note that the completeness of the LV galaxy survey in the neutral hydrogen line HI is much higher, reaching 88%. A comparison of these panels indicates the need to speed up the survey of nearby galaxies in the $H\alpha$ line to have a sufficiently complete picture of the SFR diversity in them.

2. Observations and image processing

Below we present a survey of 52 nearby galaxies, most of which were observed in the $H\alpha$ line for the first time. Some of these galaxies are likely members of the closest

neighboring group Maffei2/IC342, poorly studied due to its location in the region of strong absorption in the Milky Way; the other part is a mixture of field galaxies and members of other small groups, in particular, around NGC 672, NGC 784, and in the Orion region.

CCD images of galaxies in the $H\alpha$-line and in the continuum were obtained during observing runs from 2005 to 2009. An average seeing was $1.8''$. All the observations were performed in the Special Astrophysical Observatory of the Russian Academy of Sciences (SAO RAS) with the BTA 6-m telescope equipped with the SCORPIO focal reducer (Afanasiev et al. 2005). A CCD chip of 2048×2048 pixels provides a total field of view of about $6.1'$ with a scale of $0.18''$/pixel. The images in $H\alpha$+[NII] were obtained via observing the galaxies though a narrow-band interference filter $H\alpha(\Delta\lambda =75\text{Å})$ with an effective wavelength λ=6555Å. In order to remove the stellar continuum contribution to these images, we also observed the same ields with two medium-band filters situated on both sides from $H\alpha$: SED607 with λ=6063Å, $\Delta\lambda$=167Å, and SED707 with λ=7063Å, $\Delta\lambda$=207Å. Typical exposure times were 2×600s in $H\alpha$ and $2 \times 300s$ in the continuum. Since the range of radial velocities in our sample is small, we used the same $H\alpha$ filter for all the observed objects. Our data reduction followed the standard practice and was performed within the MIDAS package. For all the data, bias was subtracted and the images were flat-fielded by twilight flats. Cosmic particles were removed and the sky background was subtracted. The next operation was to spatially align all the images for a given object. Then the images in the continuum were normalized to $H\alpha$ images using 5–15 field stars and were subtracted. $H\alpha$ fluxes were obtained for the continuum-subtracted images, using spectrophotometric standard stars from Oke (1990) observed during the same nights as the objects. The investigation of measurement errors, brought in by the continuum subtraction, flat-fielding, and scatter in the zeropoints, has shown that they have typical values within 15%. We did not correct $H\alpha$ fluxes for the contribution of the [NII] lines, because it is likely to be small for the majority of low-luminosity galaxies in our sample. For instance, according to Equation (1B) in Kennicutt et al. (2008), a typical galaxy in our sample with the median absolute magnitude $M_B = -15^m$ has a [NII]/$H\alpha$ ratio of 1/20 which is lower than the accuracy of our measurements.

3. $H\alpha$ fluxes and SFRs

The measured integrated flux of a galaxy in the $H\alpha$+[NII] lines, calibrated according to Oke's spectrophotometric standards (and noted as $F(H\alpha)$), was expressed in units of (erg$\times$ cm$^{-2}\times$ sec^{-1}). In each case, we tried to take into account not only the sum of emission knots of the galaxy but also its diffuse emission background insofar as it was not distorted by the background subtraction errors, significant in large apertures. Due to the width of the filter used, the measured galaxy fluxes are also containing emission in the neighboring line doublet [NII]. However, according to Kennicutt et al. (2008), relative contribution of the doublet for the majority of galaxies is small, especially for dwarf galaxies. The measured $F(H\alpha)$ flux is then corrected for light absorption in the Milky Way A_B(MW) using a

technique by Schlegel et al. (1998), and for internal extinction in the galaxy itself $A_B(\text{int})$, defined as

$$A_B(\text{int}) = [1.6 + 2.8(\log V_m - 2.2)] \times \log(a/b), \tag{1}$$

if $V_m > 42.7$ km s^{-1}, and $A(\text{int})=0$ otherwise. This ratio incorporated the known fact (Verheijen 2001) that internal extinction depends not only on the inclination of the galaxy, expressed in terms of its apparent axial ratio a/b, but also on its luminosity, an indicator of which according to Tully & Fisher (1977) is the amplitude of its rotation velocity V_m. Here, the quantities a/b, V_m, and $A_B(\text{int})$ are taken from Tables 1 and 4 of the CNG. Absorption in the $H\alpha$ line was adopted as proportional to the absorption in the B-band:

$$A(H\alpha) = 0.538[A_B(\text{MW}) + A_B(\text{int})]. \tag{2}$$

Following Gallagher et al. (1984), we calculated the integrated star formation rate in the galaxy as

$$SFR(M_\odot/year) = 1.27 \times 10^9 \times F_c(H\alpha) \times D^2, \tag{3}$$

where D is the distance to the galaxy, expressed in Mpc. The validity of the linear transition (3) from the flux $F_c(H\alpha)$ to the SFR has recently been a subject of critical reviews. Pflamm-Altenburg et al. (2007) and Pflamm-Altenburg & Kroupa (2009) exhaustively argued that the canonical relation (3) underestimates the SFR value in dwarf galaxies, and the weaker the luminosity of the galaxy is, the stronger the difference is. In dwarf systems with absolute magnitude $M_B \sim -10, -12^m$, an underestimation of the SFR value may reach one to two orders of magnitude. To be pricise, in what follows we conserve the SFR estimates made under the canonical relation (3). We divided the galaxies we observed into two categories: 19 galaxies belonging to a nearby association around Maffei2/IC342 and 33 general field galaxies that include both isolated galaxies and members of multiple systems. The galaxies Maffei1, Maffei2, and their companions are obscured from us by dust clouds, which create a strong and heterogeneous absorption, reaching $A_B \sim 5^m - 7^m$. This circumstance considerably hampers the measurements of $F(H\alpha)$ fluxes and increases the errors. Moreover, the magnitude of absorption A_B itself is determined at low galactic latitudes $\mid b \mid < 5°$ with a high uncertainty.

The images of 19 galaxies from the Maffei2/IC342 group and 33 general field galaxies are represented as a mosaic in Figures 2 and 3, respectively. The left and right images of each galaxy correspond to the sum and difference of the images that have been exposed in the $H\alpha$ and in the continuum. The image scales are shown by the horizontal bars equal to 1 arcmin, and the north and east orientation is indicated in the corner by arrows.

The main characteristics of the observed galaxies are listed in Tables 2 and 3, the structures of which are identical. The table columns contain: (1) — galaxy name, (2) —

equatorial coordinates for epoch J2000.0, (3) — morphological type from de Vaucouleurs digital classification, (4) — radial velocity relative to the Local Group centroid, (5) — distance to the galaxy presented in the CNG catalog including new data from Tully et al. (2006) and Karachentsev et al. (2006), (6) — absolute magnitude in the B band from the CNG, corrected for internal and external absorption, (7) — logarithm of the hydrogen mass of the galaxy, $\log(M_{HI}/M_{\odot}) = \log F_{HI} + 2\log D + 5.37$, where F_{HI} is the flux in the HI line (in Jy km s^{-1}), and D in Mpc, (8,9) — the observed and corrected flux in the $H\alpha$ line, and (10) — integrated star formation rate in the galaxy calculated from the canonical relation (3).

4.   Comments on individual objects in the Maffei group

The structure and kinematics of the binary association of galaxies around the major spirals Maffei2 and IC342 as subgroup centers were considered by Karachentsev et al. (2003a). Most of the galaxies presented in Table 2 are physical companions of either Maffei2 or IC342, judging from their radial velocities.

KKH5, KKH6. Both dIrr galaxies are peripheral members of the association, that have probably not yet reached the virialized region around Maffei2. Their distances are measured with an accuracy of $\sim 10\%$ from the TRGB detected on the images derived with the Hubble Space Telescope (Karachentsev et al. 2003b, 2006). Both galaxies show emission knots, which are more diffuse in the case of KKH6.

Cas1 = KK19. This dIrr galaxy is located in the zone of strong absorption ($A_B = 4.4^m$), which remains yet inaccessible for determining the distance via the TRGB. Its distance as a companion of IC 342 is adopted at 3.3 Mpc. The $H\alpha$ image reveals many compact HII regions some of which are circular-shaped.

KKH11, KKH12, MB1 = KK21. All the three irregular galaxies are companions of Maffei2. Each galaxy demonstrates the presence of emission knots and filaments with the values of the total $H\alpha$ flux close to one another.

Maffei1. Maffei1 is an elliptical galaxy, the distance to which is estimated by Fingerhut et al. (2003) from the central dispersion of radial velocities. Its angular sizes, corrected for absorption $A_B = 5.05^m$, extend beyond our image frame, which created problems with background subtraction. Apart from the residues of overexposed star images, there are no visible traces of emission regions on the body of the galaxy. In the table we indicate the upper limit of its possible $H\alpha$ flux.

Maffei2. This barred spiral (Sbc) galaxy also extends beyond our image frame. Based on its apparent K_s magnitude (5.22^m) from the Two Micron All Sky Survey (2MASS) and from the width of the HI line (305 km s^{-1}), we estimated its distance as 3.1 Mpc using the infrared Tully–Fisher relation $M_K = -9.35\lg(W_{50}) + 0.75$. We obtained the total $H\alpha$ flux of Maffei2 assuming that the $H\alpha$ profile of the galaxy reproduces its brightness profile in

the K–band whereas about 50% of the luminosity appeared to be outside of our frame.

Dwingeloo2. Dwingeloo2 is an irregular galaxy in the region of strong absorption $(A_B = 5.12^m)$. A rather bright star is projected on it. The image of this star is likely screening a significant part of the galaxy's $H\alpha$ flux.

MB3 = KK22. For this dIrr galaxy, we estimated only the upper limit of its $H\alpha$ flux.

Dwingeloo1 = KK23 = Cas2. This is a spiral SBbc-type galaxy, prone to strong absorption $(A_B = 6.34^m)$. For it we adopted the mean distance of the group 3.0 Mpc, although an individual assessment of the distance from the infrared Tully-Fisher relation gives (at $K_s = 8.82$ and $W = 187$ km s^{-1}) a distance of 4.7 Mpc. Approximately 20% of the luminosity of the galaxy is beyond the range of our image.

KK35. This object looks like an isolated spot of low surface brightness at the distance of 16 arcmin from the center of IC 342. It can be a dIrr galaxy in the process of merging with the giant spiral IC342 or a stellar association on the outer spiral pattern of the galaxy. Its distance, 3.16 Mpc, determined via the TRGB, is consistent within errors with the distance of IC342 itself, 3.28 Mpc, defined via the Cepheids. As the $H\alpha$ image shows, KK35 is in a state of very active star formation.

UGCA86. This is an Sm/Im galaxy with a bright association of blue stars (VIIZw9) on the SE side. Its distance, 2.96 Mpc, measured via the TRGB (Karachentsev et al. 2006), confirms the affiliation of UGCA86 to the IC 342 companions. Compact emission knots and filaments are scattered throughout the galaxy disk, but more than half of the integrated $H\alpha$ flux comes from a powerful site of star formation, VIIZw9.

CamA = KK41, CamB = KK44. Both are dIrr galaxies of low surface brightness that show the presence of a blue stellar population in the images obtained with the WFPC2 on the HST (Karachentsev et al. 2003a). Both galaxies show small compact knots and a weak diffuse emission component in the $H\alpha$ line, which indicates a sluggish process of star formation in these systems.

NGC1569. Along with M82 and several Markarian galaxies, NGC1569 belongs to the objects of the Local Volume with the most active star formation per luminosity unit of the galaxy. An abundance of arc-like emission filaments in the periphery makes the galaxy resemble a crab. Due to significant absorption $(A_B = 3.02^m)$ the distance to NGC1569 has long remained uncertain. Recently Grocholski et al. (2008) determined its distance as 3.36 Mpc using the TRGB method.

UGCA92. This dIrr galaxy is located in the sky in the vicinity of the previous galaxy. Radial velocities and distances from the observer of UGCA92 and NGC1569 are also close. These galaxies can form a bound pair on the outskirts of the group around IC342, reminiscent of the famous pair of NGC 147 and NGC 185, which are dwarf galaxies in the neighborhood of M31. In the UGCA92 body there are groups of bright emission knots, and two arcs interlocking in the northern part of the galaxy.

NGC1560, UGCA105. These are two galaxies of late Sd and Sm types, oriented at different angles to the line of sight. Their $H\alpha$ fluxes are also approximately equal. Their characteristic features are ring-shaped HII regions, apart from which there are many compact emission knots.

5. Comments on individual objects in the field

NGC404. This is the nearest isolated lenticular galaxy of moderate luminosity. In its central part small dust clouds are visible. Del Rio et al. (2004) found an extended HI shell around NGC404, and ultraviolet observations with GALEX have identified a ring-shaped structure of young stars (Thilker et al. 2010). On our $H\alpha$ image one can see fairly bright emission in the circumnuclear region of the galaxy, as well as separate emission knots, scattered in the periphery. The integrated $H\alpha$ flux of the galaxy, shown in Table 3, does not have any contribution of distant emission knots in the HI region shell. Recently, Williams et al. (2010) presented HST/WFPC2 observations across the disk of NGC404 and studied its star formation history in detail.

AGC112521. This dIrr galaxy of low surface brightness was detected in the "blind" HI survey ALFALFA, performing with the Arecibo radio telescope (Saintonge et al. 2008). Our $H\alpha$ image of the galaxy shows only one compact emission knot, which was prevoiusly spotted by Zitrin & Brosch (2008).

KK13, KK14, KK15. These are dwarf irregular companions of the spiral galaxy NGC672, discovered by Karachentseva & Karachentsev (1998), and detected in the HI surveys by Huchtmeier et al. (2000) and in the ALFALFA. All three objects have several compact emission knots, which were also noted by Zitrin & Brosch (2008).

IC1727, NGC672. These are a pair of spiral galaxies of late types (Sm, Sd). Their distance, 7.2 Mpc, was estimated by I. Drozdovsky (private communication) from the luminosity of brightest stars. It is the distance we ascribed to the four remaining members of the NGC672 group: AGC112521, KK13, KK14 and KK15. $H\alpha$ images of both spirals exhibit many HII regions, typical for Sm and Sd galaxies. Integrated $H\alpha$ fluxes of IC1727 and NGC672 are in good agreement with the fluxes, previously measured by Kennicutt et al. (2008), but are nevertheless significantly (by two to three times) higher than the fluxes, given by Zitrin & Brosch (2008).

UGC1281, KK16, KK17. These three dwarf galaxies form a group along with a brighter Sd galaxy NGC784. Their distances were measured by Tully et al. (2006) using the TRGB method. Zitrin & Brosch (2008) imaged all four galaxies in $H\alpha$. Their descriptions of emission components in these galaxies are consistent with what we see in Figure 3. However, in the case of KK16, where only a faint diffuse emission is visible, the $H\alpha$ flux measured by us is five times higher than that obtained by Zitrin & Brosch (2008). A reason for this difference remains unclear to us.

UGC1703 = KKH9. This is a dwarf spheroidal galaxy at a distance of 4.2 ± 0.3 Mpc estimated by Rekola et al. (2005) from the fluctuations of its surface brightness. Judging from this distance, UGC1703 may either be associated with the far periphery of the dwarf galaxy group around NGC784, or belong to the rare class of isolated dSph galaxies. Our $H\alpha$ image of UGC1703 does not show any signs of emission. Table 3 indicates the upper limit of its $H\alpha$ flux.

NGC855. This isolated elliptical galaxy is similar to NGC404 in terms of luminosity and hydrogen mass. Its distance, 9.73 Mpc, was determined by Tonry et al. (2001) from fluctuations of surface brightness. Wallington et al. (1988) noted the presence of a ring-shaped HI shell around it, which is atypical for E galaxies. Our snapshot of NGC855 in the $H\alpha$ line reveals bright emission in the circumnuclear area, external parts of which are extended in the polar directions. To understand the nature of this object with hybrid properties of E and S galaxies, it is necessary to investigate its kinematics in the HI and $H\alpha$ lines.

AGC122226= KUG0243+275. This isolated blue compact galaxy was detected in the HI line in the Arecibo survey (Saintonge et al. 2008). The $H\alpha$ image shows active star formation, concentrated in several knots within the central region of this galaxy.

AGES. This dIrr galaxy was discovered as a result of the "blind" AGES survey in the HI line of the vicinity of an isolated galaxy NGC1156 (Minchin et al. 2011). Judging from its radial velocity, the AGES object is a dwarf companion of NGC1156 at the projection distance of ~ 80 kpc, if we adopt for it the same distance as that of NGC1156, 7.8 Mpc. Our image of AGES in the $H\alpha$ line reveals two diffuse HII regions with a total star formation rate of $\sim 1 \times 10^{-3} M_{\odot}$/year.

KKH18. KKH18 is an isolated dIrr galaxy, the distance to which, 4.43 Mpc, is determined via the TRGB (Karachentsev et al. 2003b). KKH18 and UGC1703 are possibly forming the eastern extension of a filament of dwarf galaxies, the dense part of which is also hosting the group around NGC784. A compact HII region and weak diffuse emission in the center are visible on the body of KKH18.

UGC2773. This is an isolated BCD galaxy in the region of significant ($A_B = 2.43^m$) absorption. Its $H\alpha$ image demonstrates many compact HII regions, as well as a considerable diffuse emission. The distance to UGC2773 is estimated by us simply from the radial velocity taking the Hubble parameter of $H_0 = 72$ km s^{-1}Mpc^{-1}. Of course, in the local universe, peculiar motions can dominate over the systematic Hubble component. However, at present there is no generally accepted model that describes the local peculiar velocity field well right taking into account the Virgocentric infall and the Local Velocity Anomaly (see details in Tully et al. 2008).

UGC2905. UGC2905 is an isolated dIrr galaxy on the southern part of which a background spiral neighbor is projected. The distance to UGC2905, 5.8 Mpc, is estimated from the brightest stars (Georgiev et al. 1997). Its $H\alpha$ image reveals several compact and diffuse HII regions.

UGC 3303. This is an isolated Sm galaxy with a bright star projected on its central part. The distance of UGC 3303 is estimated as 7.2 Mpc from the brightest stars (Makarova & Karachentsev 1998). It may be located in the periphery of a scattered association of galaxies, the brightest member of which is the Orion galaxy. The $H\alpha$ image reveals a lot of small HII regions scattered across the disk of the galaxy.

KK49 = CGCG422–003. This is a BCD galaxy in the Orion complex. Its distance is evaluated from the radial velocity. The $H\alpha$ image of the KK49 body looks granulated because of the tightly located emission knots.

Orion, An0554. These are two galaxies (Sm and dIrr) located in the Orion complex in the region of significant galactic absorption. Their distances (6.4 and 5.5 Mpc, respectively) are determined by Karachentsev & Musella (1996) from the luminosity of brightest stars. The HII regions, more abundant in the Orion galaxy in accordance with its morphological Sm type, are visible on their $H\alpha$ images. Recently, Cannon et al. (2010) carried out $H\alpha$ and VLA HI observations of the Orion galaxy and found the rotating HI disk extending far outside the optical boundary of the galaxy.

HIZOA J0630+08. This HI source detected in the survey by Donley et al. (2005) is located in a dense stellar region of the Milky Way at the galactic latitude $b = -0.9°$. On the POSS-II blue and red images, not a single galaxy is seen within the radio telescope beam ($\sim 15'$). Our $H\alpha$ image does not show an optical counterpart to this radio source either, which is most likely a dIrr galaxy of low surface brightness, weakened by absorption ($A_B = 2.95^m$).

UGC3476, UGC3600, UGC3698. These are three isolated dIrr galaxies, the distances to which are found from the brightest stars (Makarova & Karachentsev 1998). Each one of them demonstrates the presence of active star formation sites which is characteristic of isolated irregular galaxies.

UGC3755. This is a dIrr galaxy, the distance to which is measured by Tully et al. (2006) applying the TRGB. Its image in $H\alpha$ indicates active star formation, most pronounced in the western part of the galaxy.

DDO47, KK65 = CGCG087–033. These two galaxies are dwarf galaxies, forming an isolated pair with a difference in radial velocities of only 6 km s^{-1}. The distances measured by Tully et al. (2006) via the TRGB confirmed a physical relationship of these galaxies. In both galaxies there are visible compact emission regions.

KK69, KK70. KK69 and KK70 are two dwarf companions of the spiral galaxy NGC2683. Both have low surface brightness. An irregular dwarf, KK69, is characterized by a very narrow HI emission with a line width of 16.5±0.6 km s^{-1} (Huchtmeier et al. 2003). Our $H\alpha$ image shows a very red or emission star-like object within its optical boundaries. The nature of this object can be clarified by spectral observations. The dwarf spheroidal system KK70 lacks any signs of $H\alpha$ emission.

NGC2787, NGC4600. These are two isolated lenticular galaxies, the distances to which are determined from surface brightness fluctuations (Tonry et al. 2001). In both cases the central parts of galaxies are over-exposed, which makes the assessment of the flux in $H\alpha$ somewhat uncertain.

6. External comparison of $H\alpha$ fluxes

The accuracy of measurement of the $H\alpha$ flux of a galaxy, and of the SFR value determined from it, depends on many factors. If variable atmospheric conditions were successfully monitored during the observations by regular calibration using the spectrophotometric standards, the main source of errors for the $F(H\alpha)$ values is inaccurate subtraction of the sky background on the obtained images. For compact starburst galaxies these errors are negligible, but for the galaxies with weak and diffuse $H\alpha$ emission, such errors appear to reach $\sim 10 - -20\%$. Note also that some authors determine the integrated flux of a galaxy as the sum of its separate HII regions, while others also take into account the general diffuse component, which also gives rise to differences in the data they provide.

We evaluated our typical accuracy of $F(H\alpha)$ as $\sim 15\%$, or ± 0.06 dex in the logarithmic scale. However, this internal assessment needs to be subject to an independent external audit.

Among the 52 galaxies we observed there are 12 objects, in which the $H\alpha$ fluxes were measured by Kennicutt et al. (2008), and 11 galaxies observed in $H\alpha$ by Zitrin & Brosch (2008). The data on $H\alpha$ fluxes in these galaxies are presented in Table 4. In the case of Kennicutt et al. (2008), we also cite the internal flux measurement errors indicated by them.

A comparison of our $\lg F(H\alpha)$ values with the data by Kennicutt et al. (2008) yields the mean square difference $\sigma(\Delta \lg F) = 0.09$ and the average difference $\langle \lg F_{KK} - \lg F_{Ken} \rangle = +0.004 \pm 0.03$, which indicates a good agreement of independent measurements. The internal error of our measurements that we have estimated as $\sigma(\lg F) = 0.06$ is approximately the same as in Kennicutt et al. (2008) (0.058), and their quadratic sum reproduces well the mean square difference $\sigma(\Delta \lg F) = 0.09$. Note, however, that the agreement of our data with the $H\alpha$ fluxes, published by Zitrin & Brosch (2008) turned out to be much worse: $\sigma(\Delta \lg F) = 0.34$ and $\langle \lg F_{KK} - \lg F_{NB} \rangle = +0.10 \pm 0.11$.

A transition from the measured $H\alpha$ flux of a galaxy to the SFR value is accompanied by additional errors, which are usually systematic. These factors include: the contribution of the emission line [NII] in the total registered $H\alpha$ + [NII] flux, different methods of correction for internal absorption in a galaxy, uncertainty of the Galactic absorption value according to Schlegel et al. (1998) at low latitudes, underestimation of the diffuse emission component of very low surface brightness, and underestimation of possible HII regions in the distant periphery of a galaxy (the case of NGC404). Finally, as noted above, the transformation of $F(H\alpha)$ into the SFR via the linear relationship (3) can significantly (by

one to two orders of magnitude) underestimate the true star formation rate due to the simplistic notions on the initial stellar mass function in dwarf systems (Pflamm-Altenburg & Kroupa 2009).

7. Some basic scaling relations

Estimates of the global star formation rate are currently obtained for 435 LV galaxies. As it is noted by many authors (Karachentsev & Kaisin 2007; James et al. 2008; Thilker et al. 2007; Lee et al. 2009) that SFR value correlates with the integrated luminosity of a galaxy, its morphological type, color index and hydrogen mass. The data on the dependence of an SFR of a galaxy on its environment are rather contradictory (Hunter & Elmegreen 2004; James et al. 2004), but the prevailing view is that such a dependence, if it exists, is weak, i.e. the process of star formation in the galaxy is more likely driven by its internal state than by external factors. Nevertheless, there are well-known cases where a close interaction or merger of galaxies leads to a spectacular burst of star formation or, the other way around, a passage of a dIrr galaxy close to a massive spiral suppresses star formation in the dwarf system due to gas stripping from its shallow potential well.

Figure 4 represents a relation between the global star formation rate and blue absolute magnitude for 435 LV galaxies. The galaxies of different morphological types are shown by characters of different colors. Empty symbols with arrows mark the instances when only the upper limit of the SFR of a galaxy is known, determined from Equation (3). The straight line in the figure corresponds to the constant specific SFR per luminosity unit, $SSFR = 0.70 \times 10^{-10} M_\odot yr^{-1} L_\odot^{-1}$. Evidently, dwarf galaxies are systematically located below this line. According to Pflamm-Altenburg & Kroupa (2009) their deviation from the linear relation is leveled if the transition from the measured $H\alpha$ flux to the SFR is made in the light of modern ideas on the initial stellar mass function in dwarf systems. The galaxies from Tables 2 and 3 do not noticeably stand out among the rest of the objects. A distinctive feature of the $\{SFR, M_B\}$ diagram is the presence of a rather sharp upper boundary, $SSFR = 4.3 \times 10^{-10} M_\odot yr^{-1} L_\odot^{-1}$, which is mainly traced by dIrr, BCD, and Sm–Sc galaxies. Of the galaxies listed in Tables 2 and 3, UGC2773, KK35 and NGC1569 present examples of such cases. The existence of a critical upper value for the SSFR is obviously an important universal parameter, characterizing the process of conversion of gas into stars.

The distribution of LV galaxies by SFR values and hydrogen mass is presented in Figure 5, where the symbol designations are the same as in Figure 4. The dashed line corresponds to the constant specific SFR, related to the unit of hydrogen mass. The solid line shows a steeper dependence of SFR $\propto M_{HI}^{3/2}$, followed by individual emission complexes inside the galaxies (the Schmidt–Kennicutt law). According to Pflamm–Altenburg & Kroupa (2009), recalculation of SFR values for dwarf galaxies with the view of a more accurate initial stellar mass function decreases the regression slope in Figure 5 from 1.5 to 1.0.

To describe the evolutionary status of various samples of galaxies, Karachentsev & Kaisin (2007) suggested to use the diagnostic "past–future" diagram, where the dimensionless and distance-independent parameters

$$P = \log\{[\text{SFR}] \times T_0/L_K\}, \quad F = \log\{1.85M_{HI}/([\text{SFR}] \times T_0)\} \tag{4}$$

show which part of the observed stellar mass of the galaxy can be reproduced at the now observed SFR during the cosmological time T_0, and for how long the star formation can continue there with the present gas reserves of $M_{gas} = 1.85M_{HI}$. Here the factor 1.85 gives a correction for the average abundance of helium and molecular gas in the galaxy (Fukugita & Peebles, 2004). For the P parameter in expression (4), we use a known fact that the infrared K-band luminosity L_K of a galaxy reproduces its stellar mass at $M_*/L_K = 1M_\odot/L_\odot$ (Bell et al. 2003; Karachentsev & Kut'kin 2005). We adopted K_s-band magnitudes for 122 LV galaxies from the 2MASS survey (Jarrett et al. 2003). For the remaining objects we transferred their B-magnitudes into the K_s ones, using the empirical relations between the average color index $\langle B - K \rangle$ and the morphological type of a galaxy, discussed by Jarrett et al. (2003) and Karachentsev & Kut'kin (2005):

$$
\begin{array}{lll}
\langle B - K \rangle = 4.10 & \text{for} & T \leq 2 \\
\langle B - K \rangle = 4.60 - T/4 & \text{for} & T = 3 - 8 \\
\langle B - K \rangle = 2.35 & \text{for} & T = 9, 10.
\end{array}
\tag{5}
$$

The distribution of 435 LV galaxies on the "Past–Future" plane is presented in Figure 6, where galaxies of different types, (E, S0, dSph), (Sa, Sab, Sb, Sbc), (Sc, Scd, Sd, Sdm, Sm), and (Irr, BCD), are given in four separate panels. As above, open symbols with arrows indicate objects with only the upper limit of SFR or HI-flux. Here, we omitted 41 galaxies with the upper limit of both SFR and HI-flux because of their uncertain position on the F–scale.

It is easy to see that the galaxies of different morphological types occupy different regions on the $\{P, F\}$ plane, demonstrating the expected evolutionary segregation. The evolutionary trend according to galaxy types is also reflected in the data of Table 5. Its columns indicate: (1) — morphological type, (2) — number of galaxies of this type in the LV with measured SFRs, (3,4) — median values of the P and F parameters. We can draw the following conclusions from these data.

1. The current SFRs in the E, S0, and dSph galaxies can reproduce only about 2% of their stellar mass, therefore in the past their average SFR was significantly higher. Typical gas reserves in the E, S0, and dSph galaxies are rather uncertain, and their typical gas consumption timescale remains uncertain too.

2. According to the median parameters P and F, the spiral galaxies of early types, dominated by the bulges, have already passed the peak of their evolution. The past

SFR was an order of magnitude higher than the present one, and the current gas reserves can support the SFRs during merely 28% of the cosmological timescale.

3. In disk-like galaxies of the late Sc–Sm types, the current SFR is only slightly lower than it was in the past. The resources of gas in Sc–Sdm galaxies are supplying their observed SFRs during almost another Hubble time.

4. The population of Irr and BCD galaxies had almost the same mean SFR in the past, as it does now. Their gas reserves are sufficient for further star formation on a timescale of around $1.8T_0$. The diagonal character of the distribution of these galaxies on the $\{P, F\}$ plane obviously points to the variability of SFR in galaxies of low masses. Facing periodic bursts, dIrr galaxies are moving from the top left to the bottom right quadrant, acquiring the signs of BCD galaxies. Note that Stinson et al. (2007) simulated the evolution of dIrr galaxies taking into account effects of gas outflow due to the wind from SNe, and found cyclic bursts of star formation on the scale of ~ 0.3 Gyr with an amplitude of $\sim (2 - 3)^m$ for dwarf systems of very low masses.

5. Scattering of the LV galaxies on the $\{P, F\}$ diagram is quite high, reaching two to four orders of magnitude depending on the morphological type. As we already noted, the $H\alpha$ flux measurement error normally does not exceed ~ 0.1 dex, although near the detection limit these errors can be much higher. The uncertainty of transformation of $F(H\alpha)$ into [SFR], discussed by Pflamm–Altenburg & Kroupa (2009) also affects the parameter spread, but it shifts the galaxies exactly arriswise $F = -P$. Thus, much of the galaxy dispersion in Figure 6 does not have an instrumental origin, but a cosmic one. The smallest dispersion, $\sigma(P) = 0.4, \sigma(F) = 0.6$, is observed for the population of late type-spirals, Sc–Sdm. It is most likely that the rotation of Sc–Sdm galaxies and the stimulation of star formation it causes in gas-rich disks makes this process fairly regular.

8. The present cosmic SFR density

As demonstrated by Madau et al. (1996), Villar et al. (2008), Gonzalez et al. (2010), Westra et al. (2010), and other authors, the average SFR in previous epochs $z \simeq 1 - 2$ was an order of magnitude higher than nowadays. Analyzing the change in the average SFR density from redshift $\rho_{SFR}(z)$, it is important to reliably fix the current value of $\rho_{SFR}(0)$ from the observations of nearby galaxies.

To this end, we used all available data on the SFR of galaxies situated within 8 Mpc at galactic latitudes $|b| > 10°$. We did not consider more distant objects because the present completeness of the $H\alpha$ survey drops appreciably beyond 8 Mpc. The integrated SFR for the 8 Mpc sample amounts to 53 $M_\odot yr^{-1}$. As is seen from Figure 1, the present $H\alpha$ survey is quite complete up to $M_B = -15^m$. Based on the relation "SFR versus M_B" in Figure 4, we estimate that the integrated contribution of dwarf galaxies still unobserved in $H\alpha$

adds about 4 $M_\odot yr^{-1}$ to the total amount. Therefore, the mean SFR density within 8 Mpc turns out to be $\rho_{SFR}(0) = 0.032 M_\odot yr^{-1} Mpc^{-3}$. As was noted by Karachentsev & Kut'kin (2005), the mean stellar mass density within 8 Mpc, estimated from the K-band luminosity density $j_K(L \mid 8Mpc) = 6.8 \times 10^8 L_\odot Mpc^{-3}$, appeared to be (1.7 ± 0.2) times higher than the mean cosmic density $j_K(L)_{cosmic} = (3.8 \pm 0.6) \times 10^8 L_\odot Mpc^{-3}$ obtained by Cole et al. (2001) and Bell et al. (2003) from 2MASS. Reducing for the local overdensity, yields the mean cosmic density of SFR in the present epoch

$$\rho_{SFR}(0) = (0.019 \pm 0.003) M_\odot yr^{-1} Mpc^{-3}.$$

Table 6 gives a comparison of our estimate with the data obtained by other authors based on the samples of different depths and different compilation methods. As one can see, the agreement of independent estimates of $\rho_{SFR}(0)$ is quite satisfactory.

The data from Table 7, gathering the values of some basic cosmic parameters describing the star formation within 1 Mpc^3 at z=0 and h=0.72 can be useful to validate various models of galaxy evolution. The rows of the table present: (1) — the critical density of matter, (2) — the luminosity density in the K-band (also evaluating the mean density of stellar mass at $M_*/L_K = 1 M_\odot/L_\odot$), (3) — the mean density of hydrogen mass according to HIPASS (Zwaan et al. 2003), (4) — the mean density of SFR, and (5,6) — the mean density of the dimensionless parameters P and F, derived from the quantities of rows (2)–(4) via Equations (4). The value $\rho(P) = -0.17$, actually averaged with the galaxy masses proportional to their K–luminosity, means that the current star formation rate in a unit volume is only 1.5 times lower than the average SFR in past epochs. This result looks significantly at odds with the notion that the characteristic SFR in the $z \simeq 1$ era was an order of magnitude more intense than at $z = 0$. The other value, $\rho(F) = -0.50$, means that an average unit volume has such a reserve of gas in the galaxies, which is able to maintain the average present rate of star formation in them for another 4–5 Gyr. In other words, our universe has already gone more than halfway in the history of transformation of gas into stars and is now being on the descending branch of this process immediately after the era of peak intensity of star formation. It is needless to stress that this assertion is true only under the condition that the bulk of gas is located in the volume of the galaxies themselves, rather than being distributed in the intergalactic space.

9. Concluding remarks

The program of our massive $H\alpha$ survey of galaxies in the neighboring volume a radius of 10 Mpc allows us to determine some basic cosmic parameters, characterizing the rate and resource of star formation in the local universe. An important prerequisite for this is an exclusion of deliberate selection in the choice of objects for the observational program by morphological type and/or other features. A simple principle is evident here: the lower the selectivity of objects is for observations, the simpler the interpretation of the data obtained will be. The lack of accurate distance measurements to a part of nearby galaxies somewhat

blurs this ideal situation. It should be noted, however, that positions of galaxies in the diagnostic diagram {P, F} (Figure 6) do not depend on the errors of distance finding.

Keeping the E, S0, and dSph galaxies, which are not expected to have $H\alpha$ emission, in our sample we found surprisingly that in some of them the process of star formation goes on at a fairly high rate. For example, spheroidal galaxies KDG61, DDO44 and KKR25 indicate the presence of separate emission knots, in which a young stellar population is formed. The isolated E and S0 galaxies, NGC404, NGC855, and NGC4460, demonstrate active $H\alpha$ emission in their central regions, which probably indicates a constant inflow of the accreting intergalactic gas into these galaxies (Moiseev et al. 2010). There are reasons to assume that a population of young semi-formed dwarf galaxies, similar to the HI-clouds in the Virgo (122746.2 +013601) and CVnI (122043.4 +461233) clusters, or to the HIJASS (102100.2 +684200) and Leib (AGC219303) objects in the M81 and LeoI groups is located in the upper right quadrant of the diagnostic diagram (Figure 6). To clarify the nature of such objects with masses comparable to the masses of dwarf galaxies, much deeper observations are needed with flux limit of $F(H\alpha) \sim 10^{-16}$ erg/cm^{2}sec and $F(HI) \sim 10^{-2} Jy$ km/sec. Such observations would obviously require a significant amount of time on large telescopes. This demand should be related to the predictions of modern scenarios of galaxy evolution. So far, the existing shallow $H\alpha$ survey of nearby dwarf galaxies is successfully competing with another survey of these galaxies in the ultraviolet range on GALEX (Gil de Paz et al. 2003) due to weaker absorption in the $H\alpha$ line and higher angular resolution.

References

Abazajian K., et al. 2009, ApJS, 182, 543

Afanasiev V.L., Gazhur E.B., Zhelenkov S.R. & Moiseev A.V. 2005, Bull.SAO, 58, 90

Bell E.F., McIntosh D.H., Katz N., Weinberg M.D., 2003, ApJS, 149, 289

Bell E.F. & Kennicutt R.C. 2001, ApJ, 548, 681

Bouchard A., Da Costa G.S., Jerjen H., 2009 AJ, 137, 3038

Brinchmann J., Charlot S., White S.D.M., et al, 2004, MNRAS, 351, 1151

Cannon L.M., Haynes K., Most H. et al. 2010, AJ, 139, 2170

Cole S., et al. 2001, MNRAS, 326, 255

Colless M., et al. 2001, MNRAS, 328, 1039

Del Rio M.S., Brinks E., Cepa J. 2004, AJ, 128, 89

Donley J.L., Staveley-Smith L., Kraan-Korteweg R.C., et al, 2005, AJ, 129, 220

Epinat B., Amram P., Marcelin M., 2008, MNRAS, 390, 466

Fingerhut R.L., McCall M.L., De Robertis M., et al, 2003, ApJ, 587, 672

Fukugita M., Peebles P.J.E., 2004, ApJ, 616, 643

Gallagher J.S., Hunter D.A. & Tutukov A.V. 1984, ApJ, 284, 544

Gallego J., Zamorano J., Aragon-Salamanca A., Rego M., 1995, ApJ, 455, 1

Georgiev Ts.B., Karachentsev I.D., Tikhonov N.A., 1997, Astron. Lett., 23, 514

Gil de Paz A., Madore B.F. & Pevunova O. 2003, ApJS, 147, 29

Giovanelli R., et al. 2005, AJ, 130, 2598

Gonzalez V., Labbe I., Bouwens R.J. et al, 2010, ApJ, 713, 115

Grocholski A.J., Aloisi A., van der Marel R.P., et al, 2008, ApJ, 686L, 79

Hanish D.J., Meurer G.R., Ferguson H.C., et al, 2006, ApJ, 649, 150

Huchtmeier W.K., Karachentsev I.D. & Karachentseva V.E., 2003, A&A, 401, 483

Huchtmeier W.K., Karachentsev I.D. & Karachentseva V.E., 2001, A&A, 377, 801

Huchtmeier W.K., Karachentsev I.D., Karachentseva V.E. & Ehle M. 2000, A&AS, 141, 469

Hunter D.A. & Elmegreen B.G. 2004, AJ, 128, 2170

Hunter et al. 1993 AJ, 106, 1797

James P.A., Knapen J.H., Shane N.S., et al., 2008, A&A, 482, 507

James P.A., Shane N.S., Beckman J.E., et al. 2004, A&A, 414, 23

Jarrett T., Chester R., Cutri R., et al, 2003, AJ, 125, 525

Jones D.H., et al. 2004, MNRAS, 355, 747

Kaisin S.S.,& Karachentsev I.D., 2008, A&A, 479, 603

Kaisin S.S., Karachentsev I.D., 2006, Astrofizika, 49, 287

Kaisin S.S., Kasparova A.V., Kniazev A.Yu., Karachentsev I.D., 2007, Astron. Lett., 33, 1

Karachentsev I.D., 1994, Astron. Astrophys. Trans. 6, 1

Karachentsev I.D., Karachentseva V.E., Huchtmeier W.K., Makarov D.I., 2004, AJ, 127, 2031 (= CNG)

Karachentsev I.D., Kaisin S.S., Tsvetanov Z., Ford H., 2005, A&A, 434, 935

Karachentsev I.D., Kaisin S.S., 2007, AJ, 133, 1883

Karachentsev I.D., Sharina M.E., Dolphin A.E., Grebel E.K., 2003a, A&A, 408, 111

Karachentsev I.D., et al, 2003b, A&A, 398, 479

Karachentsev I.D., Dolphin A.E., Tully R.B., et al, 2006, AJ, 131, 1361

Karachentsev I.D. & Kut'kin A.M., 2005, Astronomy Lett., 31, 299

Karachentsev I.D. & Musella I., 1996, A&A, 315, 348

Karachentseva V.E. & Karachentsev I.D., 2000, A&AS, 146, 359

Karachentseva V.E. & Karachentsev I.D., 1999, A&AS, 135, 221

Karachentseva V.E., Karachentsev I.D., & Richter G.M., 1998, A&AS, 127, 409

Kennicutt R.C., Lee J.C., Funes J.G., et al. 2008, ApJS, 178, 247

Kennicutt R.C. & Kent S.M., 1983 AJ, 88, 1094

Kennicutt R.C. et al., 1989 ApJ, 337, 761

Kraan-Korteweg R.C., Tammann G.A., 1979, Astron. Nachr., 300, 181

Lee J.C., Kennicutt R.C., Funes J.G., et al. 2009, ApJ, 692, 1305

Madau P., Ferguson H.C., Dickinson M.E., et al. 1996, MNRAS, 283, 1388

Makarova L.N. & Karachentsev I.D., 1998, A&AS, 133, 181

Meurer G.R. et al. 2006, ApJS, 165, 307

Miller B.W. & Hodge P. 1994, ApJ, 427, 656

Minchin R. F., Momjian E., Auld R., et al, 2011, AJ, accepted

Moiseev A.V., Karachentsev I.D. & Kaisin S.S., 2010, MNRAS, 403, 1849

Oke J.B. 1990, AJ, 99, 1621

Perez-Gonzalez P.G., Zamorano J., Gallego J., et al, 2003, ApJ, 591, 827

Pflamm-Altenburg J., Weidner C., Kroupa P., 2007, ApJ, 671, 1550

Pflamm-Altenburg Kroupa P., 2009, ApJ, 706, 516

Rekola R., Jerjen H., Flynn C., 2005, A&A, 437, 823

Saintonge A., Giovanelli R., Haynes M.P., et al, 2008, AJ, 135, 588

Salim S., Rich R.M., Charlot S., et al., 2007, ApJS, 173, 267

Schlegel D.J., Finkbeiner D.P. & Davis M. 1998, ApJ, 500, 525

Spergel D.N., et al. 2007, ApJS, 170, 377

Stinson G.S., Dalcanton J.J., Quinn T., et al, 2007, ApJ, 667, 170

Thilker D.A., Bianchi L., Meurer G., et al., 2007, ApJS, 173, 572

Thilker D.A., Bianchi L., Schiminovich D. et al. 2010, ApJ, 714, L171

Tonry J.L., Dressler A., Blakeslee J.P., et al. 2001, ApJ, 546, 681

Tresse L., Maddox S.J., 1998, ApJ, 499, 112

Tully R.B., Shaya E.L., Karachentsev I.D. et al. 2008, ApJ, 676, 184

Tully R.B., Rizzi L., Dolphin A.E., et al. 2006, AJ, 132, 729

Tully R.B. & Fisher J.R., 1977, A&A, 54, 661

van Zee L. 2000, AJ, 119, 2757

Verheijen M.A.W., 2001, ApJ, 563, 694

Villar V., Gallego J., Perez-Gonzalez P.G., Pascual S., 2008, ApJ, 677, 169

Wallington S., Katz N., Gunn J.E., et al, 1988, BAAS, 20, 1038, 42.06

Westra E., Geller M.J., Kurtz M.J., et al, 2010, ApJ, 708, 534

Williams B.F., Dalcanton J.J., Gilbert K.M., et al. 2010, ApJ, 716, 71

Young J.S., Allen L., Kenney J.D. & Rownd B. 1996, AJ, 112, 1903

Zitrin A., Brosch N., 2008, MNRAS, 390, 408

Zwaan M.A., Staveley-Smith L., Koribalski B.S., et al, 2003, AJ, 125, 2842
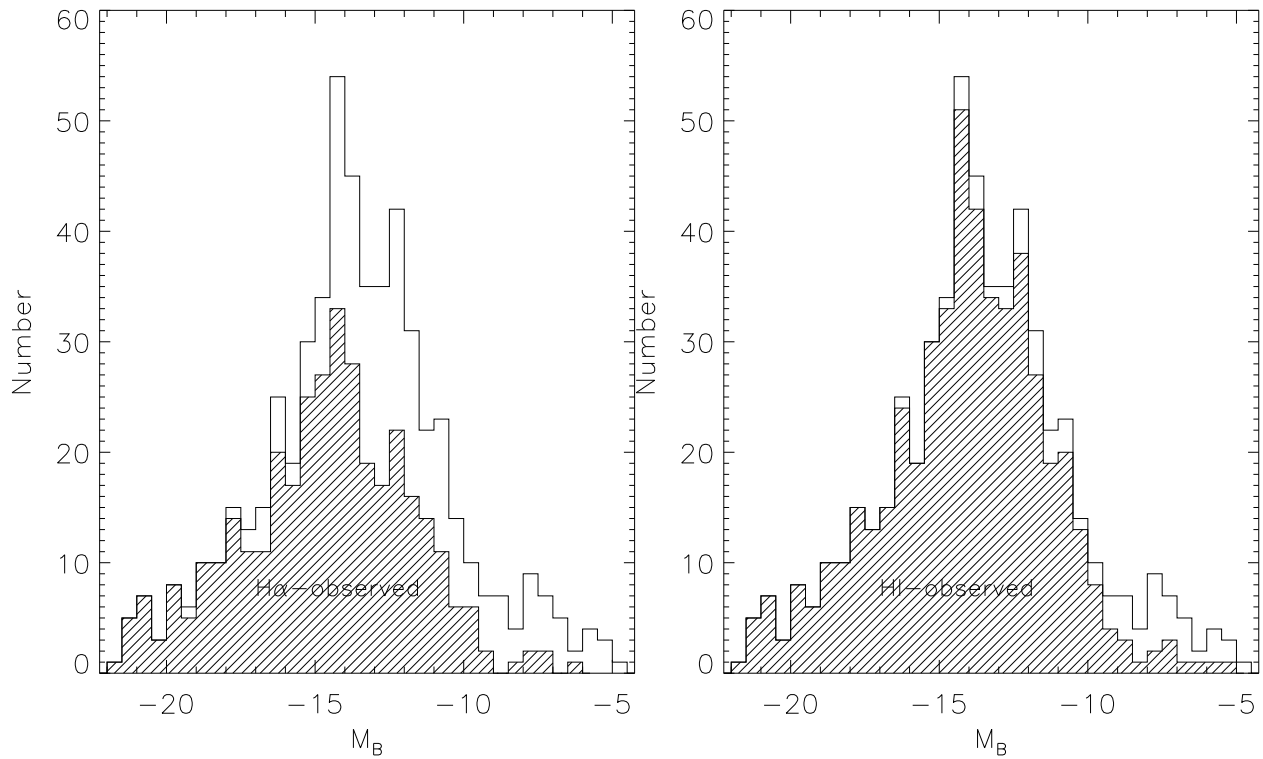
Fig. 1.— Histograms showing the fraction of the LV galaxies observed in the Hα line (left) and the HI-line (right) depending on their blue absolute magnitude.
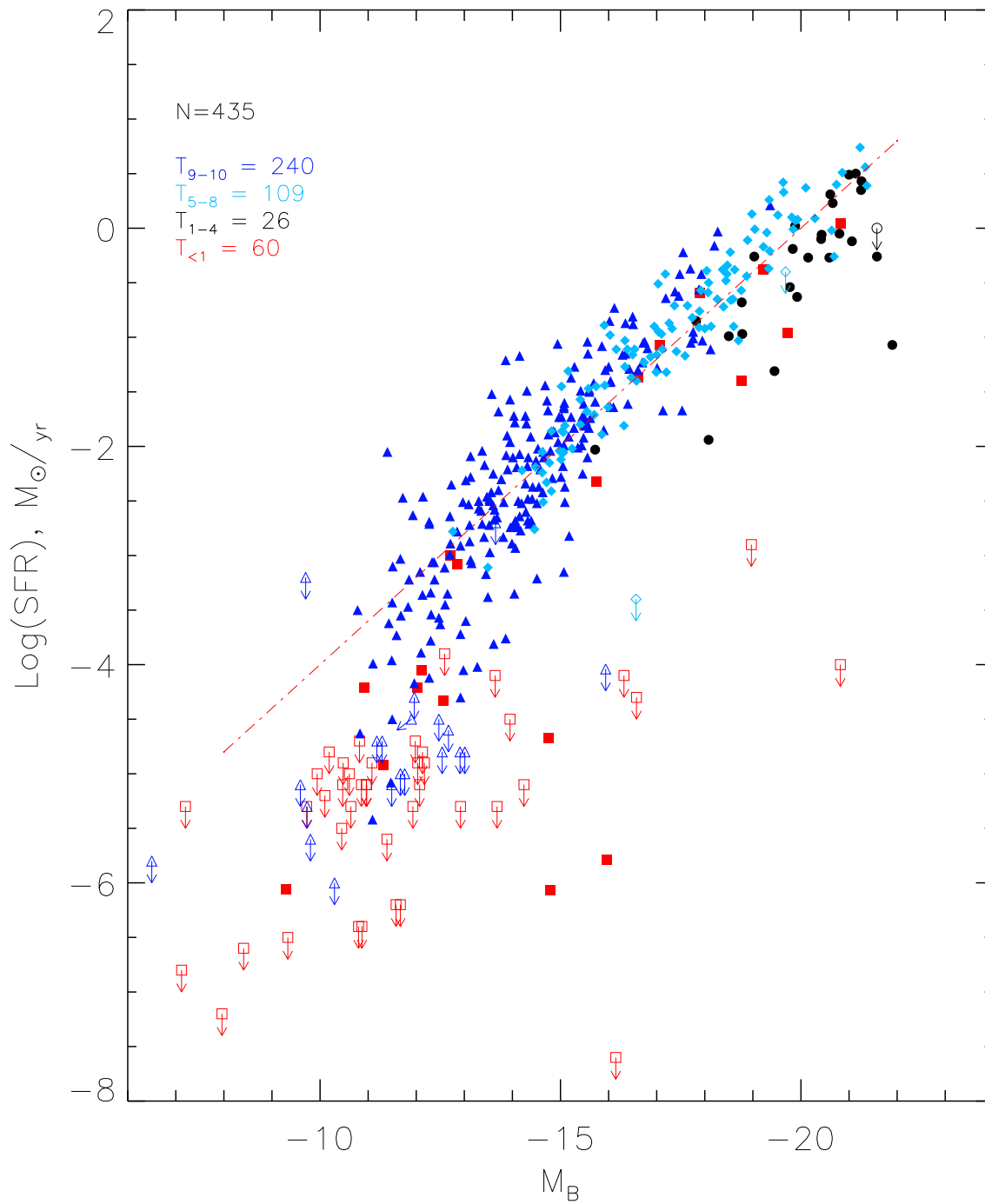
Fig. 4.— SFR vs. blue absolute magnitude for 435 LV galaxies. The open symbols indicate the galaxies with only the upper limit of their SFR. The line corresponds to a constant SFR per unit luminosity.
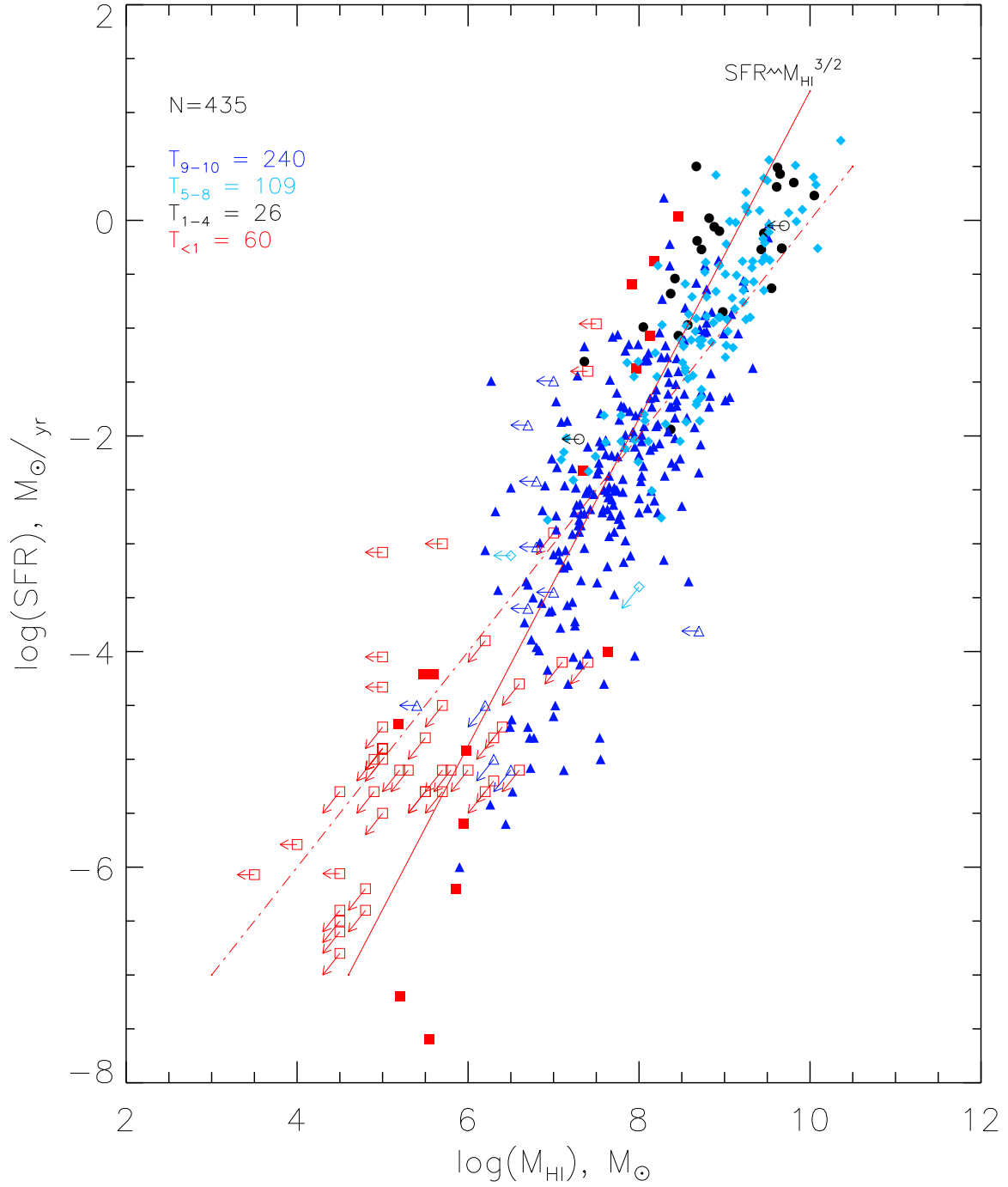
Fig. 5.— SFR vs. neutral hydrogen mass for 435 LV galaxies. The objects with an upper limit of SFR or M_{HI} are indicated by open symbols. The dashed line corresponds to a fixed SFR per unit hydrogen mass and the solid line traces the relationship SFR$\propto M_{HI}^{1.5}$.
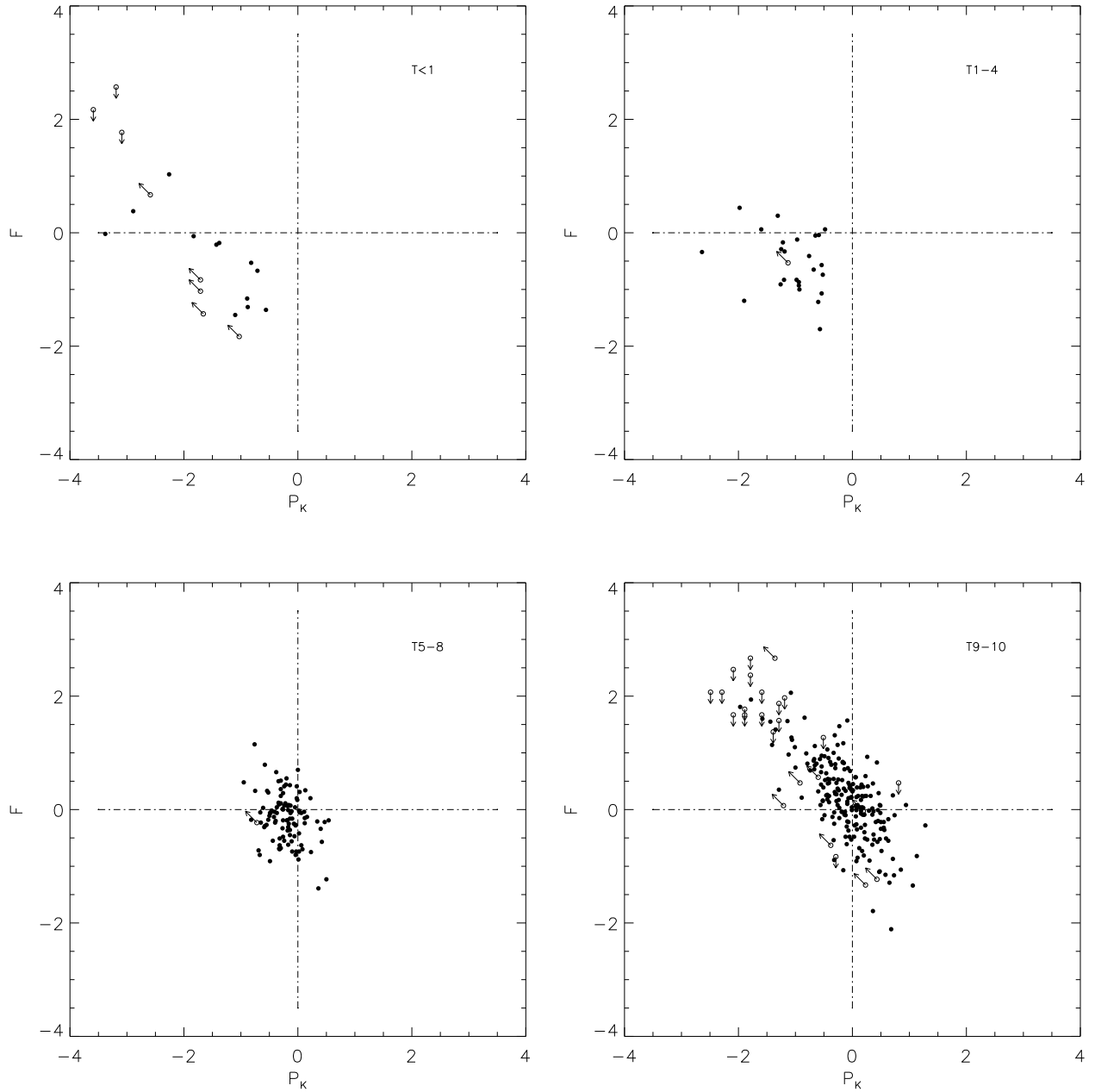
Fig. 6.— LV galaxies of different morphological types on the diagnostic diagram "Past-Future". The objects with an upper limit of SFR or M_{HI} are shown by open symbols with arrows.

Table 1: Basic contributions to the $H\alpha$ survey of the LV galaxies

Reference	N_{LV}	Sample
Kennicutt & Kent, 1983	25	Spiral,Irregular
Kennicutt et al. 1989	14	Spiral,Irregular
Hunter et al. 1993	37	Irregular
Miller & Hodge,1994	11	M81 group
Young et al. 1996	16	Spiral
van Zee, 2000	15	Isolated irregular
Bell & Kennicutt, 2001	24	Spiral,Irregular
Gil de Paz et al. 2003	10	BCD
James et al. 2004	49	S0/a–Im
Hunter & Elmegreen, 2004	50	Im, BCD
Meurer et al. 2006	10	HIPASS selected
Epinat et al. 2008	27	Spiral
Kennicutt et al. 2008	171	T> -1, B $< 15^m$, $\mid b \mid > 20°$
Bouchard et al. 2009	18	Sculptor and CenA groups
This paper	207	All types

Table 2: Galaxies in the IC342/Maffei complex

Name	RA Dec (2000.0)	T	V_{LG} km s^{-1}	D_{MW} Mpc	M_B mag	lg $M(HI)$ $M_\odot$	lg $F(H\alpha)$ erg/cm^{2}s	lg $Fc(H\alpha)$ erg/cm^{2}s	lg(SFR) $M_\odot$/yr
KKH5	010732.5+512625	10	304	4.26	-12.27	6.87	-13.31	-13.05	-2.69
KKH6	013451.6+520530	10	270	3.73	-12.38	7.12	-13.78	-13.42	-3.18
Cas1	020607.9+690036	10	284	3.3	-16.70	8.11	-12.32	-11.37	-1.24
KKH11	022435.0+560042	10	308	3.0	-13.35	7.68	-13.10	-12.64	-2.59
KKH12	022727.0+572916	10	303	3.0	-13.03	7.53	-13.11	-12.37	-2.32
MB1	023535.6+592247	10	421	3.0	-14.81	7.23	-13.37	-12.46	-2.41
Maffei1	023635.5+593918	-3	246	3.01	-18.97	–	-14.0:	-12.9:	-2.9:
Maffei2	024154.5+593611	4	212	3.1	-20.37	8.82	-11.99	-10.34	-0.35
Dwing2	025408.5+590019	10	316	3.0	-14.55	8.30	-13.52	-12.42	-2.36
MB3	025543.6+585142	10	280	3.0	-13.65	6.32	-14.0:	-12.8:	-2.7:
Dwing1	025656.1+585442	4	333	3.0	-18.93	8.63	-12.22	-10.81	-0.81
KK35	034512.6+675150	10	320	3.16	-14.30	6.27	-12.13	-11.59	-1.49
UA86	035949.5+670731	8	275	2.96	-17.95	8.79	-11.94	-11.06	-1.02
CamA	042515.6+724821	10	164	3.93	-14.06	8.22	-13.19	-12.99	-2.70
N1569	043049.1+645053	9	88	3.36	-19.36	8.29	-10.59	-9.94	0.21
UA92	043200.3+633650	10	89	3.01	-15.60	8.35	-12.30	-11.56	-1.51
N1560	043249.9+715252	7	171	3.45	-16.87	9.10	-11.60	-11.37	-1.19
CamB	045306.9+670557	10	266	3.34	-11.85	7.12	-13.56	-13.36	-3.21
UA105	051415.1+623451	8	279	3.15	-16.81	8.51	-11.58	-11.27	-1.17

Table 3: Field galaxies observed in $H\alpha$

Name	RA Dec (2000.0)	T	V_{LG} km s^{-1}	D_{MW} Mpc	M_B mag	lg $M(HI)$ $M_\odot$	lg $F(H\alpha)$ erg/cm^{2}s	lg $Fc(H\alpha)$ erg/cm^{2}s	lg SFR $M_\odot$/yr
N404	010926.9+354303	1	195	3.24	−16.61	8.02	−11.49	−11.44	−1.32
AGC112521	014107.9+271926	10	482	7.2	−11.26	6.89	−14.81	−14.74	−3.93
KK13	014216.8+262204	10	556	7.2	−13.11	7.03	−13.77	−13.69	−2.87
KK14	014442.7+271716	10	622	7.2	−12.13	7.51	−14.24	−14.17	−3.36
KK15	014641.6+264805	10	563	7.2	−11.43	6.98	−14.52	−14.44	−3.63
IC1727	014730.1+271952	8	535	7.2	−17.71	9.16	−11.94	−11.84	−1.02
N672	014753.2+272601	7	618	7.2	−18.76	9.24	−11.56	−11.39	−0.57
U1281	014932.3+323533	7	367	4.97	−15.86	8.31	−12.46	−12.37	−1.88
KK16	015520.6+275715	10	400	5.40	−12.65	6.68	−13.97	−13.91	−3.35
KK17	020009.9+284957	10	360	4.92	−11.50	6.35	−13.96	−13.91	−3.43
N784	020116.8+285037	8	386	4.97	−16.58	8.54	−11.95	−11.90	−1.40
U1703	021255.8+324851	-2	-	4.2	−11.54	6.3:	−15.2:	−15.1:	−4.7:
N855	021403.7+275238	-5	774	9.73	−17.07	8.13	−12.14	−12.05	−0.97
AGC122226	024638.9+274335	9	625	8.6	−13.13	7.56	−13.17	−13.06	−2.09
AGES	030037.0+254707	10	439	7.8	−12.33	6.20	−14.15	−13.94	−3.06
KKH18	030305.9+334140	10	375	4.43	−12.39	7.14	−13.73	−13.55	−3.16
U2773	033207.1+474737	9	397	5.5	−16.12	8.27	−11.83	−11.30	−0.72
U2905	035700.6+163128	10	344	5.8	−14.41	7.26	−13.39	−13.10	−2.47
U3303	052459.5+043018	8	446	7.2	−16.03	8.55	−11.95	−11.80	−0.98
KK49	054141.5+064054	9	376	5.2	−14.94	7.75	−12.13	−11.60	−1.07
Orion	054502.0+050406	8	276	6.4	−17.04	8.87	−12.40	−11.66	−0.95
A0554	055736.7+072931	10	340	5.5	−12.85	7.30	−13.92	−13.37	−2.79
HIZOA	063009 :+082237	10	259	3.6	−9.7:	7.17	−14.0:	−13.4:	−3.2:
U3476	063029.2+331807	10	477	7.0	−14.27	8.15	−12.74	−12.52	−1.73
U3600	065540.0+390542	10	435	7.3	−13.53	7.84	−13.52	−13.44	−2.61
U3698	070918.8+442248	10	464	7.2	−14.30	7.78	−13.03	−12.94	−2.13
U3755	071351.8+103119	10	190	6.98	−15.53	7.89	−12.64	−12.56	−1.77
DDO47	074155.0+164802	8	160	7.98	−16.04	9.06	−12.57	−12.54	−1.64
KK65	074231.2+163340	10	168	7.62	−14.29	7.55	−12.69	−12.66	−1.79
KK69	085250.7+334752	10	419	7.7	−11.96	7.59	−15.2:	−15.2:	−4.3:
KK70	085522.0+333333	-3	-	7.7	−11.86	6.8:	−15.3:	−15.2:	−4.4:
N2787	091918.6+691212	1	838	7.48	−18.50	8.05	−12.54	−12.33	−1.49
N4600	124023.0+030704	1	648	7.35	−15.72	7.3:	−12.86	−12.83	−2.00

Table 4: External comparison of the measured $H\alpha$ fluxes

Galaxy	log(F)		
	This paper	Zitrin & Brosch 2008	Kennicutt et al. 2008
A112521	−14.81	−14.36	−
KK13	−13.77	−13.41	−
KK14	−14.24	−14.53	−
KK15	−14.52	−14.48	−
IC1727	−11.94	−12.27	−11.96±.06
N672	−11.56	−12.00	−11.49±.06
U1281	−12.46	−12.65	−12.45±.07
KK16	−13.97	−14.76	−
KK17	−13.96	−14.03	−
N784	−11.95	−11.66	−11.78±.04
N855	−12.14	−12.29	−12.23±.04
Maffei2	−11.99	−	−11.95±.06
UA86	−11.94	−	−12.01±.07
N1569	−10.59	−	−10.62±.01
UA92	−12.30	−	−12.52±.03
N1560	−11.60	−	−11.54±.05
UA105	−11.58	−	−11.60±.03
DDO47	−12.57	−	−12.51±.06

Table 5: Median parameters for different morphological samples

Type	(T)	N	P	F
E,S0,dSph	(<1)	20	−1.7:	−0.4:
Sa–Sbc	(1–4)	26	−0.95	−0.55
Sc–Sm	(5–8)	108	−0.15	−0.10
Irr,BCD	(9–10)	240	−0.15	+ 0.25

Table 6: Total SFR density in the Local universe ($z = 0$, $H_0 = 72$ km s^{-1} Mpc^{-1}, extinction corrected)

$\log(\rho_{SFR})$ $M_\odot$/yr/Mpc^3	Reference	Note
-1.95 ± 0.04	Gallego et al. 1995	emission line galaxies
-1.73 ± 0.07	Tresse & Maddox 1998	I–band survey
-1.64 ± 0.02	Perez-Gonzalez et al. 2003	optically–selected
-1.66 ± 0.08	Brinchmann et al. 2004	SDSS–based
-1.81 ± 0.03	Hanish et al. 2006	HI– selected
-1.75 ± 0.03	Salim et al. 2007	UV–based
-1.72 ± 0.08	James et al. 2008	$H\alpha$ Local universe
-1.72 ± 0.06	This paper	$H\alpha$ Local Volume

Table 7: Some cosmic density parameters

Parameter	Quantity	Reference
ρ_c	$1.43 \cdot 10^{11} M_\odot$/Mpc^3	Spergel et al. 2007
$j_K(L)$	$3.8 \cdot 10^8 L_\odot$/Mpc^3	Cole et al. 2001, Bell et al. 2003
$\rho(HI)$	$0.44 \cdot 10^8 M_\odot$/Mpc^3	Zwaan et al. 2003
$\rho(SFR)$	$0.019\ M_\odot$/yr Mpc^3	This paper
$\rho(P)$	-0.17	This paper
$\rho(F)$	-0.50	This paper